

# On Entrainment Rates in Nocturnal Marine Stratocumulus

By BJORN STEVENS<sup>1,2\*</sup>, DONALD H. LENSCHOW<sup>2</sup>, IAN FALOONA<sup>2</sup>, C-H. MOENG<sup>2</sup>, D. K. LILLY<sup>3</sup>,  
B. BLOMQUIST<sup>4</sup>, G. VALI<sup>5</sup>, A. BANDY<sup>4</sup>, T. CAMPOS<sup>2</sup>, H. GERBER<sup>6</sup>, S. HAIMOV<sup>5</sup>, B. MORLEY<sup>2</sup>,  
D. THORTON<sup>4</sup>

<sup>1</sup>*Department of Atmospheric Sciences,  
University of California Los Angeles, Los Angeles California, USA*

<sup>3</sup>*National Center for Atmospheric Research  
Boulder CO, USA*

<sup>3</sup>*School of Meteorology  
University of Oklahoma, Norman OK, USA*

<sup>4</sup>*Department of Chemistry  
Drexel University, Philadelphia PA, USA*

<sup>5</sup>*Department of Atmospheric Science  
University of Wyoming, Laramie WY, USA*

<sup>6</sup>*Gerber Scientific Inc., Reston, Virginia, USA*

8th November 2002

## SUMMARY

The first research flight (RF01) of the second Dynamics and Chemistry of Marine Stratocumulus (DYCOMS-II) field study is analyzed. The data attracted our interest because they showed a consistently deepening cloud layer despite macroscopic conditions which previous work has suggested should be an indication of cloud thinning or break up. Detailed analysis of the flight data shows that despite the cloud top entrainment instability parameter being well beyond its critical value the cloud did indeed deepen through the night. Our best estimates show little indication of rapid changes in cloud top, while cloud base was found to be lowering at a rate of several meters per hour. This evolution, and independent measurements of trace-gas budgets, imply an entrainment rate of  $0.004 \pm 0.001 \text{ ms}^{-1}$ . This is compared to entrainment rates from recently proposed parameterizations (forced by the observed forcing of the cloud layer) which range from 0.002 to  $0.008 \text{ ms}^{-1}$ . Of the five parameterizations we test at least two are clearly not plausible. One of the remaining three yield estimates near the bounds of the observational uncertainty, and while plausible probably need adjusting. The other two agrees well with the data, although at least one of them exhibits peculiar sensitivities. Large-eddy simulation of this case was able to reproduce the macroscopic evolution of the layer, but in doing so had some difficulty in maintaining the observed mixing line structure at cloud top. A comparison of the observed and simulated turbulent structure show these to be broadly consistent, although there is an indication that the intensity and structure of the simulated turbulence differ from the observations near the flow boundaries, particularly at cloud top.

KEYWORDS: Mixing Clouds Boundary Layers

## 1. INTRODUCTION

In commenting on attempts to relate the entrainment rate to the turbulent structure of the active fluid O. M. Phillips (1966) writes: “It has, indeed, almost acquired the status of a hoary old chestnut.” Although the intervening decades have brought more and better experiments, new observations, and the advent of simulation, this view has tended toward confirmation. Indeed, accompanying the proliferation of new data one finds a steady march of new problems for which entrainment is a critical process. For instance, our inability to quantify (let alone understand) entrainment greatly hinders our ability to understand the dynamics of the stratocumulus-topped boundary layer (STBL); moreover, the inability of large-eddy simulation to resolve the processes at the entrainment interface undermines our confidence in its ability to accurately simulate entrainment (*cf.*, Lilly, 1968; Moeng *et al.*, 1996; Bretherton *et al.*, 1999, Stevens 2002).

\* Corresponding author: Department of Atmospheric Sciences, University of California Los Angeles, 405 Hilgard Ave., Box 951565, Los Angeles, CA 90095-1565. Email: bstevens@atmos.ucla.edu.

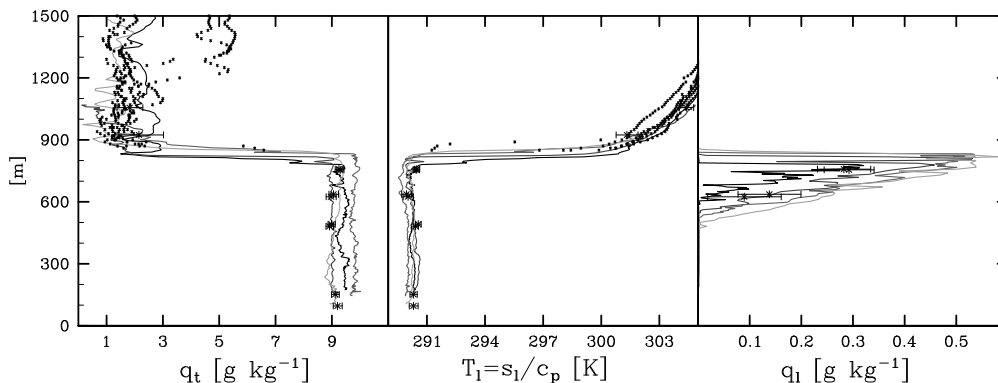


Figure 1. Cloud layer state as observed during RF01. From left to right, total water specific humidity,  $q_t$ , liquid-water static energy temperature,  $s_l/c_p$ , and liquid water specific humidity,  $q_l$ . Lines are from soundings, darker indicating earlier, filled circles and bars denote level leg means and standard deviations, and dots denote dropsonde data from the above-cloud portion of the descent.

New data, from a set of field observations collectively referred to as the second study of the Dynamics and Chemistry of Marine Stratocumulus (DYCOMS-II), were collected to address these issues (Stevens *et al.*, 2002). DYCOMS-II took place during July 2001, in the heart of the Northeast Pacific stratocumulus regime, approximately 500 km west-southwest of San Diego, California. Major features of the DYCOMS-II strategy relevant to this study were: (i) primarily nocturnal flights; and (ii) long constant-altitude legs flown along 60 km diameter circles at a variety of levels from which the state of the stratocumulus-topped boundary layer (STBL) and its turbulent statistics could be sampled *in situ*, and cloud and surface properties could be sampled remotely. Collecting primarily nocturnal data greatly facilitates an analysis of the energetics of the layer, which is difficult to estimate in the highly evolving diurnal situation for which almost all previous data have been collected. In characterizing the turbulent state of the layer, DYCOMS-II flights also collected high-rate dimethyl sulfide (DMS) and ozone ( $O_3$ ) data. These trace gases have special properties which make them well suited as tracers of entrainment and thus complement heat and moisture-budget based estimates of this important quantity (Lenschow, *et al.*, 1999). The remote sensing capabilities of the aircraft which included dropsondes, lidar, and millimeter cloud radar (Vali *et al.*, 1998), greatly extended the effective sampling volume of the measurements, so that cloud evolution could be tracked even when the aircraft was not in the cloud layer. Lastly, long periods in the target area helped reduce uncertainties associated with sampling errors.

In sum DYCOMS-II consisted of nine research flights, six of which were nocturnal and incorporated flight patterns well suited to the goals of this study. In this paper, however, we focus on only the first of these six flights, Research Flight 1 (RF01). Our attention was drawn to this case because the cloud layer showed clear evidence of significant deepening throughout the flight, despite macroscopic conditions which many believe should be indicators of cloud break up.

These points are roughly illustrated in Fig. 1, where we show successive soundings made in the study area through the course of the flight, and estimates of the state of the STBL at specific heights as derived from thirty-minute flight-legs flown at constant altitude. Here the state of the layer is indicated by values of the total water specific humidity,  $q_t$ , liquid water specific humidity,  $q_l$ , and the liquid water static energy

temperature, i.e.,  $T_l \equiv s_l/c_p = (Tc_p + gz - Lq_l)/c_p$ , where  $s_l$  is the liquid water static energy,  $g$  is the gravitational acceleration,  $z$  is height above the surface as measured by the aircraft radar altimeter,  $T$  is the ambient temperature,  $L = 2470 \text{ KJ kg}^{-1}$  is the latent heat of vaporization, and  $c_p = 1015 \text{ J kg}^{-1} \text{ K}^{-1}$  is the isobaric specific heat of moist air. Both  $q_t$  and  $s_l$  (alternatively,  $T_l$ ) are effectively adiabatic invariants of the moist system. Striking elements of this figure include: the extent to which the layer is well mixed; the stationarity of the free-troposphere over the nearly eight hours between the first and last sounding; and the apparent thickening of the cloud with time.

The cloud layer is also unstable according to the theory of cloud-top entrainment instability (CTEI) developed by Randall (1980) and Deardorff (1980). This theory posits that whenever

$$\kappa \equiv 1 + \frac{\Delta s_l}{L\Delta q_t} > \kappa_*, \quad (1)$$

mixtures of air from the free-tropospheric and from the cloud layer will be negatively buoyant, promoting enhanced mixing and the dissolution of the cloud. Essentially,  $\kappa$  (which we define above in terms of  $s_l$  and  $q_t$ ) measures the importance (from the perspective of buoyancy) of evaporative cooling versus warming for mixtures of cloudy and clear air. Thus  $\kappa > \kappa_*$  says that the evaporative cooling is sufficient to make at least some mixtures of clear and cloudy air negatively buoyant with respect to the cloud layer. For conditions encountered during DYCOMS-II  $\kappa_* \approx 0.23$ . At a glance,  $\Delta s_l \approx 10150 \text{ J kg}^{-1}$ , and  $\Delta q_t \approx -7.5 \text{ g kg}^{-1}$ , which yields a value of  $\kappa \approx 0.45$ , which is significantly larger than  $\kappa_*$ .

Although past observations (e.g., as summarized by Kuo and Schubert, 1988, also see preliminary analysis of RF03 from DYCOMS-II by Gerber et al., 2002) have provided little support for CTEI, recent modeling studies have helped revive the concept. Two-dimensional simulations by Bretherton and MacVean (unpublished manuscript, 1999) show that, in the absence of other processes,  $\kappa > \kappa_*$  is a sufficient condition for cloud dissolution. Three dimensional studies (Lock and MacVean 1999) which examine the energetics of CTEI also indicate that  $\kappa > \kappa_*$  is a sufficient condition for energy to be produced by mixing at cloud top. Large-eddy simulation by Moeng (2000) finds that in cloud layers whose state and forcings are more similar to what is typically observed there is no evidence of an energetic contribution from CTEI. However, both Moeng (2000) and Lewellen and Lewellen (1998) find that in simulations with  $\kappa > \kappa_*$ , cloud fractions fall below unity and the cloud liquid water path is precipitously reduced. For these reasons the belief, particularly within the modeling community, that CTEI is a fundamental parameter regulating cloud evolution has remained—notwithstanding the observational record.

This state of affairs motivates us to look a bit deeper into the RF01 data from DYCOMS-II, with the following questions in mind: Did the cloud layer really deepen this much? If so, does the apparent instability of the layer, as measured by the Randall-Deardorff CTEI criterion, stand up to more careful analysis? In either case, what were the entrainment rate and energetics of the layer during RF01 of DYCOMS-II and how well are these captured by simple entrainment rate parameterizations and/or large-eddy simulation?

## 2. BOUNDARY LAYER STRUCTURE AND EVOLUTION

In addressing questions such as those above, one typically thinks in terms of the Lagrangian evolution of a mixed layer embedded in a uniform and stationary environment. Such a framework is the basis of most theoretical and numerical analysis.

Although such a restricted view is not necessary, it does make things easier. For instance the assumption of the STBL being well mixed allows one to track the evolution of the STBL state by making measurements anywhere within the layer. By focusing on the Lagrangian evolution one can neglect the effects of horizontal advection, and hence the problems associated with determining it. And to the extent to which environmental properties are slowly changing, or better yet constant, one can deduce these with a relatively small number of measurements — thereby facilitating the use of a single aircraft whose measurements are concentrated within the mixed layer. For these reasons it makes sense to first evaluate the extent to which these conditions are met. We first focus on the question of the constancy of the environment; the extent to which the STBL measurements sample the Lagrangian evolution of a mixed layer are discussed thereafter.

(a) *Macroscopic environment*

From the point of view of the STBL, those aspects of the environmental state whose constancy one would most like to establish are: the heat and moisture fluxes at the surface, the radiative fluxes at the top of the layer, and the thermodynamic properties of the air overlying the layer. Given the uniformity in the cloud field as seen by satellite toward the end of the flight (left panel, Fig. 2), one can at least entertain hope of a reasonably uniform large-scale environment.

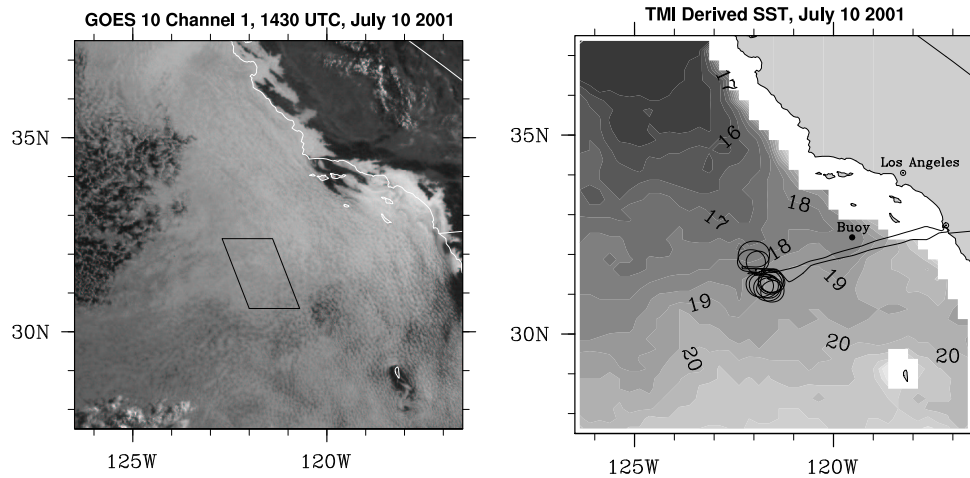


Figure 2. Left panel: GOES-10, Channel 1 Reflectance, from 14:30 UTC (7:30 am local time) on July 10, 2001, with target area boxed. Right panel: sea-surface temperatures for July 10, as derived from the TRMM (Tropical Rainfall Measurement Mission) Microwave Imager with the RF01 flight-track superposed. The numbers denote surface temperatures along contours which are sometimes difficult to distinguish.

The most important potential source of surface flux variability is a change in the sea surface temperature as the STBL advects downstream. Winds during RF01 were slightly over  $7 \text{ m s}^{-1}$  out of the west-northwest, which means that over an eight hour measurement interval the STBL would advect downstream approximately 200 km. Fortunately there was no indication that SSTs varied substantially over the target area. Based on satellite imagery (e.g., Fig. 2) and an analysis of the radiometric surface temperatures measured by two probes mounted under the aircraft fuselage, the sea surface temperatures varied by about 0.5K over the bulk of the study area (although

the totality of measurements sample a wider range of values, i.e., 1 - 1.5 K), with warmer water to the south-east. Although there is a tendency for the surface to warm as one advects downstream, our later analysis of the temporal evolution of the STBL state shows that this warming is commensurate with the warming and moistening of the layer as it advects downstream. As a result downstream variations in surface fluxes can be expected to be within the uncertainty of our estimates of the mean.

Even for a perfectly Lagrangian flight, wind shifts across the top of the STBL, and shear in the wind profile in the free-troposphere can lead to situations whereby the air-mass overlying the STBL at the end of the flight was one to two hundred kilometers away at the beginning of the flight. Changes in the state of the free troposphere can affect the radiative flux at the top of the STBL and the properties of the air being entrained. Despite clear windshifts across the top of the STBL (with the free-tropospheric wind being more westerly) Fig. 1 indicates that the air immediately above the STBL remained remarkably constant in its thermodynamic properties. Among all of the DYCOMS-II flights, RF01 was perhaps the best behaved in this respect, which was one reason for selecting it for this study.

There is an elevated moist layer evident in two of the soundings in Fig. 1 (both from dropsondes during the last leg), which, although it shows little sign of directly interacting with the STBL, might be expected to modify the radiative forcing at the top of the layer. It turns out that this layer was evident in almost all of the soundings, albeit at heights above 1500 m and hence not apparent in Fig. 1. The one exception was along the northernmost portion of the first flight leg, which appeared to be under drier air throughout the troposphere. This apparent north-south gradient in upper-level precipitable water is consistent with TMI ([Tropical Rainfall Measurement Mission] Microwave Imager) retrievals (not shown). Nonetheless, all lines of evidence suggest that for the data we analyze below (which tended to be to the south of those initial soundings), an elevated moist layer containing 3-5mm of precipitable water was always present. Calculations with the Fu and Liou (1993)  $\delta$ -four stream radiative transfer code using the observed state, but with moist layers similar to those observed inserted at altitudes ranging from 1200-2200 m, indicate that while the moist layer significantly affects the radiative forcing at the top of the cloud layer, the exact altitude of this layer has a relatively small effect (i.e.,  $\pm 10\%$ ). Thus we conclude that, at least from the perspective of the upper boundary, conditions were also relatively constant throughout the flight.

### (b) *Lagrangian Analysis*

Given the apparent homogeneity in the upper and lower boundaries of the STBL, conditions during RF01 would appear ideal for Lagrangian flight maneuvers. However, Fig. 2 shows that this goal was not always realized. If it had been, we would have seen the locus of center points from the different circles tracing a trajectory from the west-northwest following the mean wind. This roughly holds for the first three circles, but a navigation error as we started the fourth circle led us to fly the remaining circles approximately 60 km downstream of the target air-mass. Some of this was mitigated in the last four circles, whereby to stay out of a military warning area the aircraft backtracked slightly to the northwest.

To illustrate the effects of these excursions in Fig. 3 we plot  $\mathbf{x}_0$  the position of the STBL air-column sampled during each flight circle according to where we estimate it to have been at some common time,  $t_0 = 9300$  s after take off. This time was chosen to equal the mid-point time of the first boundary layer flight circle. If we had been flying a perfectly Lagrangian track we would expect all of the flight circles to overlay one

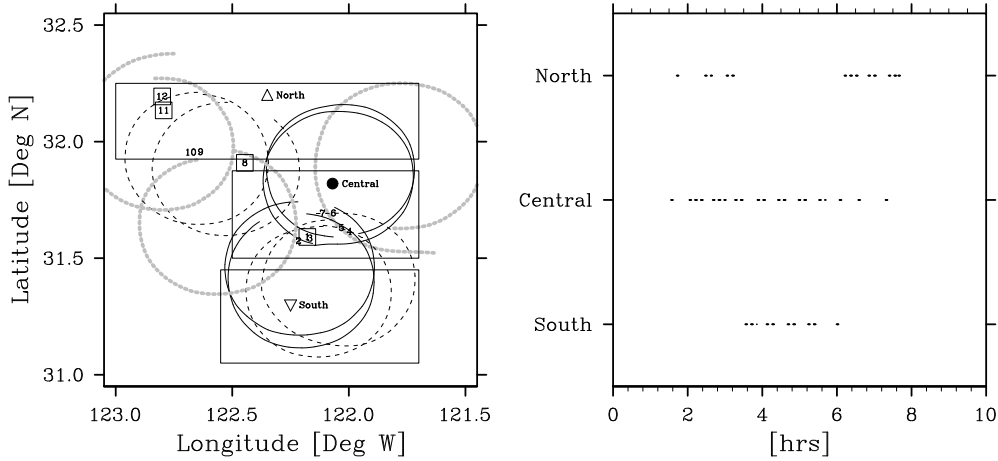


Figure 3. Left Panel: Estimated position of STBL air-masses (as sampled along circular flight-paths) at  $t = t_0$ . Solid black circles denote cloud legs, dashed black circles denote legs in subcloud layer. Thickened gray circles denote flight legs above the STBL. Order and position of aircraft soundings are denoted by numbers (Note that soundings 1, 2 and 3 are very near each other in the center of the plot, and soundings 9 and 10 also are adjacent to one another.) The boxed numbers (1, 8, 11, 12) indicate the four soundings which extended through the depth of the STBL and are plotted in Fig. 1. The large boxes denote three study regions: central, north and south. Right Panel: Short blackened intervals indicate the time spent in one of three study regions.

another identically. To make this figure we estimate the mean vector wind  $\mathbf{U}$  and its time variation  $\partial\mathbf{U}/\partial t$  from all the circles flown in the STBL, and then adjust the vector position of the air mass  $\mathbf{x}$  at some time  $t$  to its estimated position,  $\mathbf{x}_0$  at time  $t = t_0$ , according to:

$$\mathbf{x}_0 = \mathbf{x} - \mathbf{U}(t - t_0) - \frac{1}{2} \frac{\partial\mathbf{U}}{\partial t} (t - t_0)^2. \quad (2)$$

This method is not perfect: turbulent fluctuations in the wind lead to diffusion of the air mass, and estimates of  $\partial\mathbf{U}/\partial t$  are compromised by spatial variability in the observed wind. Nonetheless it gives a reasonable idea of how the air mass is sampled.

This analysis suggests that by separately considering the evolution of three regions (north, south and central) some of the effects of deviating from a Lagrangian flight plan can be mitigated. Because the central region is best sampled in both space and time, we focus our attention there. Although the subsequent analysis is based on this three region breakdown we also considered other breakdowns, for instance a five region breakdown with a smaller central region. This analysis did not yield important new information; i.e., it did not produce systematic east-west variability, and it had less data in each region.

By segregating data according to whether it fell in the north, south, central, or none of the regions, and assuming that the layer is well mixed in terms of adiabatically invariant quantities (so we can treat measurements at all heights equivalently) we can evaluate the Lagrangian evolution of important state variables in the STBL (technical details of this and subsequent analysis of the aircraft data are discussed in appendix A; our methods for estimating uncertainty are discussed in appendix B). This is shown in Fig. 4 for  $s_l$  and  $q_t$ . The data suggest  $1.7 \pm 0.26 \text{ g kg}^{-1} \text{ d}^{-1}$  of moistening and about  $1.9 \pm 0.3 \text{ K d}^{-1}$  of warming of the STBL as it advects downstream over warmer water. These are not too different from what one would expect if the air-sea temperature and moisture differences remained fixed (*cf.*, Fig. 2).

Segregating data by Lagrangian region also allows us to separate spatial and temporal derivatives, with the former being indicated by systematic differences among the study regions. Although the data indicate clear temporal trends in  $q_t$  and  $s_l$ , only  $s_l$  shows obvious latitudinal gradients, with cooler air to the north. These gradients tend to be somewhat larger than what we would expect based on the Lagrangian changes of  $s_l$  estimated above. The lack of a discernible latitudinal gradient in  $q_t$  may reflect its longer adjustment timescale as predicted by mixed layer theory,<sup>†</sup> or the obscuration of a signal by larger meso-scale variations.

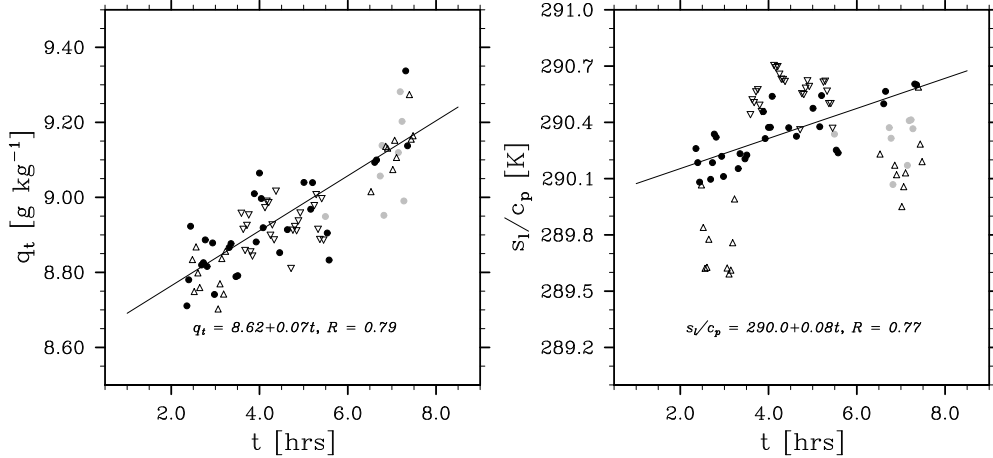


Figure 4. Estimated temporal variation of  $q_t$  (left panel) and  $s_l/c_p$  in the STBL derived from 2.5 minute averages of state variables measured along boundary layer legs during RF01. Note that the regression lines are fit only to data (solid circles) taken in the central region. Data taken in the northern, southern regions are denoted by upper, lower pointing triangles, respectively. Data which did not fall in a study region are denoted by gray circles.

At temperatures and pressures characteristic of the middle of the STBL,  $dq_s/dT \approx 0.7 \text{ g kg}^{-1} \text{ K}^{-1}$ . This implies that if  $s_l$  and  $q_t$  are changing at the same rate,  $dq_s/dt$  (which is just  $(dq_s/dT)dT_l/dt$ ) will be less than  $dq_t/dt$ ; hence from a saturation point of view moistening of the STBL dominates over warming and we expect the change in the mean state to be accompanied by a slight lowering of cloud base with time. This is indeed evident in Fig. 5 where the lifting condensation level (LCL) is plotted along with cloud base as determined from aircraft soundings. The gradual lowering of cloud base predicted by changes in the LCL is also evident in the sounding data. The consistency between LCL estimates of cloud base and the measured cloud base from aircraft penetrations also supports the mixed layer assumption made in our initial analysis. The data also show a consistently lower cloud base to the north, consistent with the latitudinal changes in  $s_l$  discussed above. Because the latter soundings, plotted in Fig. 1, tended to preferentially be in the northern study area, the profile data exaggerate the lowering of cloud base. Nonetheless, to the extent that these data indicate a trend they indicate that cloud base is lowering. This is opposite to what proponents of CTEI would have predicted given the observed value of  $\kappa$ .

<sup>†</sup> Schubert *et al.*, (1979) show that the adjustment time of moist static energy  $h = s_l - Lq_t$ , and  $q_t$  are commensurate. However, because  $h$ , depends linearly on  $q_t$ , their analysis does not clearly separate temperature and moisture. Repeating it in terms of  $s_l$  and  $q_t$  shows the latter to have a longer adjustment time.

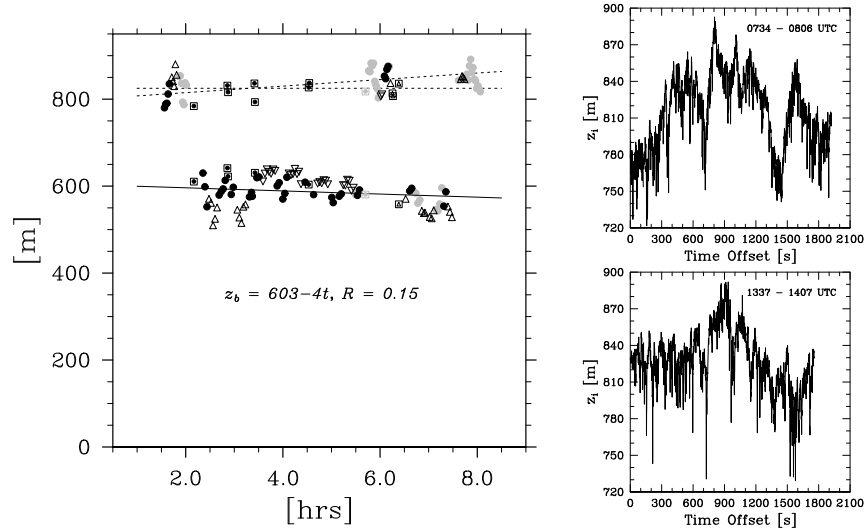


Figure 5. Estimated temporal variation of cloud-boundaries. Level leg data are used to calculate LCL which is plotted following the symbol convention of previous figures, sounding data are indicated with open squares, filled with a region indicator symbol. Cloud top is estimated from soundings and radar/lidar retrievals. The radar and lidar retrievals are averages over sub-intervals and identified by study region. Examples of the 1 second lidar estimates of cloud top, from the first and last lidar leg, are shown in the two right panels. In the left panel, the regression on points in the central study region is used to estimate the evolution of cloud base, and two lines are drawn by eye to indicate the plausible evolution of cloud top. One corresponds to no change in time, the other to a value of  $dz_t/dt$  of  $7.5 \text{ m hr}^{-1}$  ( $2.1 \text{ mm s}^{-1}$ ).

The evolution of cloud top during the course of the flight is much more difficult to assess. Unlike cloud base, for which we had measurements (or proxies) for nearly the entire flight, continuous estimates of cloud top only occurred over three intervals, and these tended to measure cloud depth in different Lagrangian regions. If variability in the cloud top was confined to small spatial scales (order kilometers) this might not be a problem. However, in addition to illustrating the uniformity of cloud coverage the lidar returns in the right panels of Fig. 5 indicate considerable mesoscale variability in cloud height. Any spatial coherence in these patterns is not readily discernible and thus difficult to attempt to correct for. This degree of variability, and the failure of the cloud top measurements to sample the same air mass make it difficult to put meaningful bounds on the change in cloud top height through the course of the flight. For this reason no attempt was made to fit lines to the cloud top height data, and instead fits were drawn by eye as a means of evaluating the plausibility of varying scenarios. Fortunately, our inability to be more quantitative in this respect does not undermine our ability to constrain the thermodynamic budgets.

Thus while the cloud boundary data suggest that the cloud layer is probably deepening as it advects downstream, it remains to be seen if the layer truly satisfies the CTEI criterion as set forth by Randall (1980) and Deardorff (1980). To address this question Fig. 6 shows the data from all cloud-top penetrations plotted in  $q_t, T_t$  space. It shows that at least within the central study region, the data lie on a mixing-line well on the unstable side of the neutrally stable mixing line. Along one of the cloud penetrations which occurred outside the central study region there is evidence that the aforementioned elevated moist layer actually intersected the cloud layer, leading to a region whose mixing line was slightly stable with respect to CTEI. However this appears

to be an isolated case, as other soundings outside the central study region lie on the same mixing line as the data within the central region. Thus we conclude that for the most part the boundary layer air, whose evolution we analyze, was mixing with air in the free-troposphere whose mixing ratio was about  $1.5 \text{ g kg}^{-1}$  and whose effective temperature ( $s_l/c_p$ ) was 300-301 K. This implies  $\Delta q_t = 7.5 \pm 0.5 \text{ g kg}^{-1}$  and  $\Delta s_l = 10150 \pm 1015 \text{ J kg}^{-1}$  — values commensurate to what one would have estimated from Fig. 1 and unequivocal in their satisfaction of the CTEI criterion.

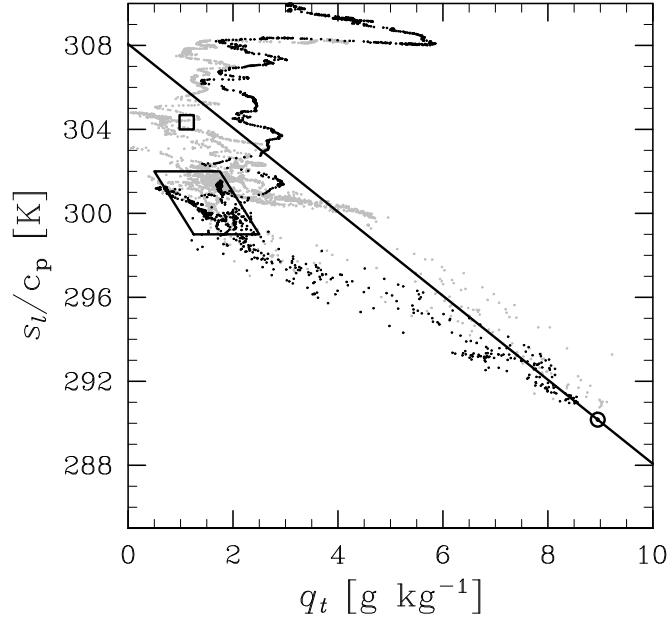


Figure 6. Plot of 2.5Hz data (i.e., fast 25 Hz data sub-sampled every fifth point) showing  $(q_t, s_l/c_p)$  from all cloud penetrations during RF01. Black symbols indicate that sample is drawn from central region, other symbols indicate data from cloud penetrations elsewhere. Circle marker in lower right shows best estimate of STBL state from Fig. 4, rhomboid shows estimated properties of free tropospheric air which is ultimately mixing with air from the STBL, small square (near 304 K) shows properties of free-troposphere as deduced from a level leg flow near 1050 m. Free-tropospheric states to the left of the solid line denote layers whose value of  $\kappa$  are greater than  $\kappa_*$ , and hence unstable according to the classical formulation of CTEI.

In summary, this more careful analysis of the RF01 data does support the idea that the cloud layer was indeed unstable with respect to CTEI, yet still deepened — both through a lowering of cloud base and a rising of cloud top.

### 3. ENTRAINMENT RATE ESTIMATES

If one defines entrainment as the mixing of air from the quiescent free troposphere into the STBL one can quantify its rate (a velocity) in a variety of ways. To do this, consider the general equation for the expected value of a scalar (denoted by an overbar, with primes denoting deviations therefrom) in a turbulent flow

$$\frac{\partial \bar{\phi}}{\partial t} + \bar{w} \frac{\partial \bar{\phi}}{\partial z} = - \frac{\partial}{\partial z} [\psi \phi' + F_\phi] + S_\phi, \quad (3)$$

where  $\psi_\phi \equiv \overline{w'\phi'}$  is the turbulent flux,  $F_\phi$  is the vertical component of some flux (which acts on the scalar through its gradient, e.g., radiation or precipitation when  $\phi = s_l$ ), and  $S$  is some generalized source term, e.g., for reacting gases. By integrating (3) from a height  $z_{i-} \equiv z_i - \epsilon$ , just below the top of the layer, to a height  $z_{i+} \equiv z_i + \epsilon$ , just above the top of the layer, it is straightforward (*cf.*, Lilly, 1968, Stevens 2002) to show that if  $\epsilon$  is sufficiently small compared to  $z_i$

$$\left( \frac{dz_i}{dt} - \overline{w}(z_i) \right) \Delta \overline{\phi} = -\psi_\phi(z_{i-}) - \Delta F_\phi. \quad (4)$$

Here  $z_i$  denotes the base of the temperature inversion, equivalently the top of the cloud layer,  $\epsilon$  can be thought of as being on the order the undulation depth of cloud top, and  $\Delta$  denotes a difference in a quantity measured at  $z_{i+}$  and  $z_{i-}$  respectively.  $\epsilon$  can be estimated from the lidar data in Fig. 5. For 5 km subsegments  $z_i$  has a standard deviation of 13 m which roughly doubles as the subsegment length increases to 50 km. In both cases this is much less than the mean depth of the layer, so the small  $\epsilon$  assumption implicit above is warranted. In (4)  $dz_i/dt - \overline{w}$  denotes the diabatic growth rate of the layer; i.e. the entrainment velocity  $E$ , which is necessary to close a bulk formulation of the mixed layer.

This discussion leads to two methods for estimating  $E$ . One, which we call the ratio method, estimates  $E$  as:

$$E = \frac{\psi_\phi(z_{i-}) - \Delta F_\phi}{\Delta \overline{\phi}}, \quad (5)$$

the other, which we call the difference method, estimates  $E$  kinematically as

$$E = \frac{dz_i}{dt} - \overline{w}. \quad (6)$$

Because the mean subsidence velocity valid at cloud top, i.e.,  $\overline{w}(z_i)$ , is difficult to measure, we focus on the ratio method for now. An advantage of this method is that it holds for every scalar that satisfies (3). Moreover, for scalars whose greatest source of uncertainty is the kinematic flux at  $z_i$ , multiple estimates of  $E$  can be obtained by estimating the flux using independent means. For instance given  $F_\phi$ ,  $\psi_\phi(z_{i-})$  can be estimated either by eddy correlation or from a budget residual (*cf.*, Russell *et al.*, 1999). For the latter we obtain,

$$\psi_\phi(z_{i-}) = -z_i d\overline{\phi}/dt + \psi_\phi(0) - [F_\phi(z_{i-}) - F_\phi(0)] + \int_0^{z_{i-}} S_\phi dz, \quad (7)$$

which requires estimates of  $d\overline{\phi}/dt$ , as well as contributions to  $\phi$  from source and surface fluxes. In some cases each of these terms can be estimated using slow response instruments. In contrast, eddy-correlation-based estimates of  $\psi_\phi(z_{i-})$  always require fast sampling capability. Moreover, the flux needs to be estimated directly at the entrainment interface. In practice the need to sample directly at  $z_{i-}$  can be avoided by estimating  $\psi_\phi$  at multiple levels through out the STBL (including near the surface), and then using the fact that in quasi-steady state  $\psi_\phi + F_\phi$  must be linear<sup>‡</sup> through the layer, to extrapolate the profiles to  $z_{i-}$ . As discussed by Stevens *et al.*, (2002), the flight plans during DYCOMS-II, and the package of airborne instrumentation, were designed specifically around these objectives, thus allowing for optimal estimates of  $E$ .

<sup>‡</sup> Strictly speaking this is only true if  $\partial S_\phi / \partial z$  is negligible, which is thought to be the case for the scalars we consider.

With these points in mind we first examine the heat and moisture budgets, which are strongly constrained by the previous analysis of cloud base, to estimate  $\bar{E}$  using (5) and (7). Due to the absence of both sunlight and appreciable drizzle during RF01, the only diabatic term which must be considered is that due to the flux of radiant energy at long wave lengths,  $F_{lw}(z)$ .

For the surface fluxes, eddy correlation estimates extrapolated to the surface yield sensible and latent heat fluxes of  $7 \pm 10$  and  $115 \pm 14 \text{ W m}^{-2}$  respectively. The large uncertainty in the sensible heat fluxes arises because we need to extrapolate the sum of the radiative and kinematic heat fluxes to the surface, and both the radiative and kinematic fluxes have large uncertainties in the cloud layer. § If we instead calculate the surface sensible heat fluxes by extrapolating only the below-cloud measurements to the surface we arrive at a similar mean estimate which has considerably reduced uncertainty, but which is valid for a more limited time window.

We have also estimated the surface fluxes using the TOGA-COARE bulk flux algorithm (Fairall *et al.*, 1996, version 2.5b). As input to this algorithm we assumed that the mean state over the central study region, derived from Fig. 4 and tabulated in Table 1, was valid at a height of 50 m. The SST used in this was taken from a composite of radiometric surface temperatures estimated during flight periods (both soundings and level legs) in the sub-cloud layer. These measurements yield values systematically 0.5 K warmer than the satellite estimates, which is in the range of uncertainty of the two methods. Based on this input the algorithm predicts surface sensible heat fluxes of  $17 \pm 3 \text{ W m}^{-2}$  and latent heat fluxes of  $115 \pm 15 \text{ W m}^{-2}$ , which are reasonably consistent with the direct estimates.

Table 1. BEST ESTIMATES OF MEAN STATE

SST	292.5 K
$z_i$	840 m
$s_l/c_p$	290.4 K
$q_t$	$9.0 \text{ g kg}^{-1}$
$\bar{w}$	$6.00 \text{ m s}^{-1}$
$\bar{v}$	$4.25 \text{ m s}^{-1}$

To estimate the radiative forcings, which enter into the budget of  $s_l$ , we used a radiative transfer model forced by the observed state of the atmosphere. In principle measurements could be used, but using the models allows us to better evaluate the detailed vertical structure of the profile. The degree to which the model introduces possible errors can moreover be checked by comparing the measurements to the model at levels where we have data. In these calculations the mean STBL state and the surface temperatures were given the values in Table 1. These implied a cloud base of 600 m and a cloud top liquid water content of  $0.54 \text{ g kg}^{-1}$ . Above regions for which we had *in situ* data (typically above 3 km depending on sounding level) we used the 00 Z July 10 San Diego sounding blended to the McClatchey mid-latitude summer atmosphere between 10 and 15 km. Above the STBL we evaluated radiative fluxes for mean state profiles as provided by all of the soundings. Because the free-tropospheric temperature varied little among the measurements, the radiative calculations were not sensitive to which profile

§ For the radiative fluxes we use fluxes calculated from a radiative transfer code (see below) and estimate the uncertainty as the change in the radiative flux over a 50m interval centered at the measurement height.

we used. Thus to simplify matters we fit the synthetic profile:

$$T_l = \begin{cases} 297.5 + (z - z_i)^{1/3} & : z_i < z < z_* \\ 297.5 + \gamma(z - z_*) & : z_* < z \end{cases}, \quad (8)$$

where  $\gamma = 3.5 \text{ K km}^{-1}$  and  $z_* = z_i + (3\gamma)^{-3/2} \approx 1770 \text{ m}$  is chosen to match lapse rates at  $z_*$ . For the moisture profile above  $z_i$  we specified a background profile of  $q_t = 1.5 \text{ g kg}^{-1}$  with an additional moist layer whose magnitude of

$$1.5 + 4.0 \left(1 - \frac{z - 1200}{1000}\right) \text{ g kg}^{-1} \quad \text{for } 1200 \text{ m} < z \leq 2200 \text{ m} \quad (9)$$

was smoothed with a 1-2-1 filter in the vertical (where the grid spacing in the calculation was 8.4 m in the mixed layer and approximately 200 m in the vicinity of the moist layer) before being added to the background value. Although not shown, the fit for  $T_l$  agreed remarkably with the sounding data, and the fit for moisture captured the essence of the elevated moist layer, e.g., Fig. 7.

Results of radiative calculations based on this profile are also illustrated in Fig. 7. The measured and calculated profiles of radiative fluxes agree quite well, with the major point of disagreement being the downwelling component along the cloud top leg, and perhaps the upwelling component just above cloud top. From the perspective of a mixed layer model (and the heat budget estimates of entrainment), the most important quantity is the radiative flux divergence across the STBL, i.e.,  $F_{lw}(z_{i+}) - F_{lw}(0)$ . It is approximately  $50 \pm 5 \text{ W m}^{-2}$ . Note that from the bottom left panel the radiative flux jump across cloud top is  $\approx 70 \text{ W m}^{-2}$ , which is compensated for by warming associated with  $\approx 20 \text{ W m}^{-2}$  of flux convergence concentrated near cloud base.

Based on these estimates of the diabatic and surface fluxes, and previous estimates of other terms (and their uncertainties) entering into the budget-based equations for  $E$  we can estimate  $E$ , and its uncertainty, from the moisture budget as:

$$E = \frac{z_i \frac{dq_t}{dt} - \psi_{q_t}(0)}{\Delta q_t} = 0.31 \pm 0.08 \text{ cm s}^{-1}. \quad (10)$$

From the heat budget we estimate:

$$E = \frac{z_i \frac{ds_l}{dt} - \psi_{s_l}(0) + (F_{lw}(z_{i+}) - F_{lw}(0))}{\Delta s_l} = 0.47 \pm 0.08 \text{ cm s}^{-1}. \quad (11)$$

Techniques for estimating the uncertainties (which here are limited to random sampling, rather than systematic errors) in various quantities are discussed in Appendix B. In this case, the uncertainty in  $E$ , denoted  $\sigma_E$ , is predominantly due to uncertainties in estimates of the surface (and, in the case of  $s_l$ , radiative) fluxes. Uncertainties associated with the jumps and the time rate-of-change terms are smaller but still significant.

In this case, the uncertainty in  $E$ , denoted  $\sigma_E$ , is predominantly due to uncertainties in estimates of the surface (and, in the case of  $s_l$ , radiative) fluxes, uncertainties associated with the jumps and the time-rate of change terms are smaller, but similar magnitude.

The potential for large uncertainties in any individual estimate of  $E$  was a primary motivation for DYCOMS-II, where the strategy was to obtain multiple independent estimates to help us bound our uncertainty, as well as give us some indication of possible systematic errors. Toward this end we have also estimated the entrainment rate using direct estimates of the turbulent fluxes at the top of the STBL for,  $q_t$ , DMS, and  $O_3$ .

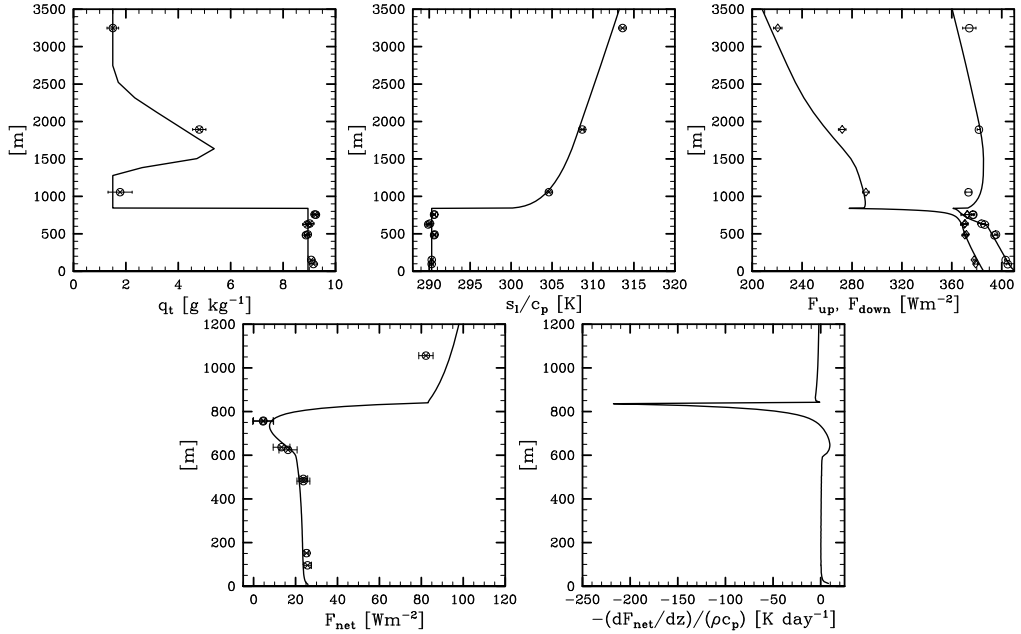


Figure 7. Plot of idealized soundings used to drive radiative calculations, and resulting radiative fields:  $q_t$  (upper left);  $s_l$  (upper center),  $F_{lw}^\downarrow$  and  $F_{lw}^\uparrow$  from calculations (lines) and measured (diamonds and circles respectively) upper right; net flux (lower left); heating rate (lower right). Note the different vertical scale on the lower plots.

Of these both  $q_t$  and  $O_3$  have been used as tracers of entrainment before, e.g., during DYCOMS-I (Kawa and Pearson, 1988), but the use of DMS is new. Because of its unique biogeo- and photochemical properties (*cf.*, Lenschow *et al.*, 1999), DMS was thought to be ideally suited to entrainment estimates in the STBL environment. This helped to motivate the development of a fast DMS sensor. The sensor performed well, and DMS behaved as expected. For instance because of its short lifetime it was not detected above the boundary layer, but was very evident within the STBL, leading to well-defined local jumps across cloud top. What was surprising, and complicated its interpretation, was large horizontal variability ( $\pm 25\%$ ) on the mesoscale (e.g., Stevens *et al.*, 2002) within the STBL. This variability also projects on the DMS flux plotted in Fig. 8. For this reason, and because  $q_t$  and  $O_3$  were relatively well behaved above the STBL during RF01, the absolute accuracy of DMS-derived estimates of entrainment was not appreciably greater than other estimates during RF01. Nonetheless it does provide an independent estimate which in itself helps reduce the uncertainty.

Fluxes of  $q_t$ , DMS and  $O_3$  are plotted in Fig. 8, and the values of  $E$  they imply are tabulated, along with previous budget estimates of  $q_t$  and  $s_l$  in Table 2.¶ For these estimates we used fast data collected in all Lagrangian regions; efforts to sort the flux data by region (as was done for the mean state data) did not lead to better behaved estimates. To estimate,  $E$  from these fluxes, we estimated the jumps as:  $\Delta q_t = 7.5 \pm 0.5$   $\text{g kg}^{-1}$ ,  $\Delta DMS = -60.2 \pm 4.5$  pptv and  $\Delta O_3 = 23 \pm 4.3$  ppbv (appendix B details

¶ We could have performed budget estimates for  $O_3$  and DMS as well, however, unlike  $q_t$  and  $s_l$  their values are not constrained by the variation of cloud base. Thus estimates of time-derivative terms are more difficult, making the budget method even more uncertain.

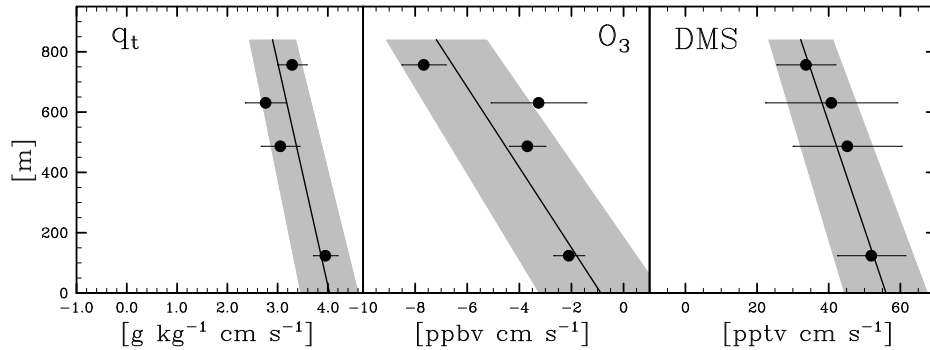


Figure 8. Flux versus height and weighted least-squared linear fit, with uncertainty shaded, for  $q_t$  (left);  $O_3$  (center); DMS (right).

how these calculations were made). For the case of DMS almost all of the contribution to  $\sigma_{\Delta DMS}$  is from variability within the boundary layer, while variability above the STBL explains most of  $\sigma_{\Delta O_3}$ . The consistency of the various estimates is rather satisfactory, encouraging us to construct a best estimate from the mean of the individual estimates weighted by their uncertainty. Such a procedure yields  $E = 0.40 \pm 0.03 \text{ cm s}^{-1}$ . Here it should be emphasized that the uncertainty (order 10%) includes only the contribution from random sampling errors. To the extent that systematic errors influence the estimates one would expect to see this in the range of magnitudes for different estimates of  $E$ . However, the consistency among the estimates suggest that they are not a major factor.

Indeed one can use the scatter of the individual estimates of  $E$  as a measure of the systematic error in the various measurements. For sake of argument, if we assume that the systematic error is randomly distributed among the techniques it can be estimated as the standard deviation of the different estimates of  $E$ , which is  $0.1 \text{ cm s}^{-1}$ . For this reason, and because values of  $E$  greater than  $0.5$  and less than  $0.3 \text{ cm s}^{-1}$  lead to an evolution of cloud base that is difficult to justify with the existing data, we believe that increasing the uncertainty in the estimate of  $E$  to  $0.1 \text{ cm s}^{-1}$  appropriately accounts for any additional uncertainties associated with unknown systematic errors.

As a further check on the above estimates we can calculate the implied subsidence rate kinematically as  $\bar{w}(z_i) = E - dz_i/dt$ . If from Fig. 5 we estimate that  $dz_i/dt \approx 0.1 \pm 0.15 \text{ cm s}^{-1}$  this implies that  $\bar{w}(z_i) = -0.30 \pm 0.16 \text{ cm s}^{-1}$ . We can also estimate  $\bar{w}(z_i)$  by assuming that the temperature profile in the few hundred meters above the cloud layer is in a radiative subsidence balance, i.e., by assuming that advection by the horizontal winds plays no role in the equation for  $s_l$  so that  $\rho \bar{w} = (\partial F_{lw}/\partial z)(\partial s_l/\partial z)^{-1}$ . Such a procedure yields a value of  $\bar{w}(z_i)$  of about  $-0.35 \pm 0.1 \text{ cm s}^{-1}$ , which is consistent with our kinematic estimate of  $\bar{w}(z_i)$ . However, given that our estimate of  $dz_i/dt$  is not strongly constrained by the data, this corroboration is illuminating only insofar as it does not show any gross inconsistencies.

#### 4. ENTRAINMENT RATE PARAMETERIZATIONS (RULES)

In this section we compare our estimates of  $E$  with those predicted from a variety of entrainment rate parameterizations (or rules for short) as reviewed by Stevens (2002). For reference three of these rules [i.e., AL, Lock (1998); CM, Moeng (2000); DL, Lilly (2002)] are fits one way or another to LES data. What we call the NT rule was proposed

Table 2. ENTRAINMENT VELOCITY ESTIMATES

Method	Estimate [ $\text{cm s}^{-1}$ ]
$q_t$ budget	$0.31 \pm 0.08$
$s_l$ budget	$0.47 \pm 0.08$
$q_t$ cloud-top flux	$0.39 \pm 0.06$
$\text{O}_3$ cloud-top flux	$0.31 \pm 0.09$
DMS cloud-top flux	$0.53 \pm 0.08$
Weighted Average	$0.40 \pm 0.03$

by Turton and Nicholls (1987) on the basis of aircraft data — here it is evaluated with two different buoyancy reversal coefficients ( $a_2 = 60$  as first suggested by Turton and Nicholls, or  $a_2 = 30$ , as is sometimes used in the literature). We also review a rule which we call LL (following Lewellen and Lewellen, 1999). The LL rule was not specifically discussed by Stevens *et al.*, (2002), because previous considerations of it depend on a characterization of the radiative flux divergence across cloud top which has yet to take a testable expression. Here, we avoid this shortcoming by simply neglecting this cloud-top term. In this case the parameterization adjust the rate of entrainment so that the net rate of working is a fixed fraction ( $1 - \eta$ ) of the flux one would find in a non-entraining PBL with identical surface and radiative forcings, *cf.*, Stevens (2002). Lewellen and Lewellen have suggested values of  $\eta$  between 0.25 and 0.30. Here we consider the case for  $\eta = 0.25$ .

To apply the rules we use the basic state specified in Table 1 and a specified radiative flux divergence of  $50 \text{ Wm}^{-2}$ . The surface fluxes in these estimates are calculated using a bulk aerodynamic formula with the estimated SST and a bulk aerodynamic coefficient of 0.0011. The value of this coefficient was taken to match the surface layer analysis of the previous section, although because of different treatments of heat and moisture fluxes in the full algorithm, this approach slightly overestimates (by  $\approx 2 \text{ Wm}^{-2}$ ) the sensible heat flux at the expense of the latent heat flux. In addition to deriving entrainment estimates for RF01, we also examined three extreme scenarios to help illustrate the sensitivity (or lack thereof) of the models. These scenarios were for a moist free atmosphere (i.e.,  $q_t(z_{i+}) = 5 \text{ g kg}^{-1}$ ), no radiative forcing (i.e.,  $\Delta F = 0$ ), and a neutrally stratified air-sea interface (i.e., SST = 290.4 K). For the case of a moist free atmosphere we chose  $q_{t+} \equiv q_t(z_{i+}) = 5 \text{ g kg}^{-1}$ , so that  $\kappa = 0$ . Hence this case illustrates the extent to which rules are sensitive to CTEI. Changing the surface temperature (which reduces sensible heat flux from 19 to  $0 \text{ Wm}^{-1}$  and latent heat flux from 113 to  $73 \text{ Wm}^{-2}$ ) or the radiative forcings exposes the sensitivities of the rules to different forcings. Results are tabulated in Table 3.

Table 3. ENTRAINMENT VELOCITY ESTIMATES IN  $\text{CM S}^{-1}$  FROM DIFFERENT ENTRAINMENT RULES.

Model	Base Case		Test Cases		
	$E$	$E_{\Delta s_l=11}$	$E_{\Delta F=0}$	$E_{q_{t+}=5.0}$	$E_{SST=290.4}$
AL	0.23	0.20	0.08	0.21	0.16
CM	0.45	0.41	0.03	0.45	0.41
DL	0.56	0.46	0.18	0.40	0.43
NT ( $a_2 = 60$ )	0.81	0.65	0.36	0.59	0.54
NT ( $a_2 = 30$ )	0.57	0.46	0.25	0.43	0.38
LL $\eta = 0.25$	0.46	0.37	0.20	0.28	0.31

Based on the RF01 data it seems difficult to defend the results of either the AL or the NT (with  $a_2 = 60$ ) rules. By using a smaller value of  $a_2$  the NT rule becomes more plausible. The DL rule behaves very similarly to the NT rule with  $a_2 = 30$ . Because both explicitly factor in buoyancy reversal they are rather sensitive (relative to the other rules) to the implied value  $\kappa$  as either increasing  $\Delta s_l$  by 10 % or decreasing the magnitude of  $\Delta q_t$  leads to marked changes in the entrainment rate. Although as currently formulated they seem to over-estimate entrainment, to the extent that our analysis over-estimates  $\kappa$ , their predicted values of  $E$  become increasingly plausible. Both the LL and CM rule are quite close to the consensus estimate of  $E$  although the CM rule predicts a seemingly unreasonable value of  $E$  (given the observed surface moisture, and hence implied incloud buoyancy fluxes) for the hypothetical case of  $\Delta F = 0$ . In many respects the LL rule exhibits sensitivities similar to those of the NT and DL rules, however it has the advantage of having only one free parameter and being conceptually rather more simple. This analysis suggests that because of their varied sensitivities, there is hope for narrowing the range of plausible rules by comparing their predicted entrainment rates to observations from DYCOMS-II flights for which the radiative forcing was less dominant, or for which  $\kappa$  took smaller values.

## 5. LARGE EDDY SIMULATION

In addition to evaluating entrainment rules, many of which have been calibrated on the basis of Large Eddy Simulation (LES), it is interesting to also test LES directly. Toward this end LES was performed using the NCAR-LES (as described by Moeng, 2000) based on an initial state taken directly from the above analysis. Because the LES code of Moeng uses only approximate thermodynamic relations,  $q_t$  and  $s_l$  were adjusted from the values specified in Table 1 so as to preserve the depth of the cloud layer. Specifically, the initial cloud top is set to  $z_{i0} = 817$  m, slightly lower than the observed height. Below  $z_{i0}$ ,  $q_t$  is set to  $8.75 \text{ g kg}^{-1}$  and  $s_l$  to  $288.7$  K. Above  $z_{i0}$ ,  $q_t$  is set to  $1.5 \text{ g kg}^{-1}$  and  $s_l$  to  $296.7 + (z - z_{i0})(1/3)$  K. This setup gives room for the LES code to spin up from a non-turbulent state to a fully turbulent state that starts with reasonable cloud base, cloud top, and inversion strength. Because the LES code is based on the Boussinesq approximation, with a constant basic state density,  $\rho = 1 \text{ g kg}^{-1}$ , boundary and radiative fluxes also had to be appropriately adjusted (i.e., by specifying them in terms of kinematic, rather than energetic, values). To mimic the surface forcings estimated from the observations this resulted in specifying  $\overline{w'T'} = 0.015 \text{ K ms}^{-1}$  and  $\overline{w'q'_t} = 0.04 \text{ g kg}^{-1} \text{ m s}^{-1}$  at the surface. For the radiative forcing a simple exponential decay parameterization was used, i.e.,

$$F_{lw}/(c_p\rho) = F_0 \left[ 1 - \exp\left(-\int_z^\infty kq_l dz\right) \right]. \quad (12)$$

Here  $F_0 = 0.05 \text{ Km s}^{-1}$  was chosen to reflect the mean flux divergence across the STBL and  $k = 130 \text{ g m}^{-2}$  was chosen in accord with previous experiments. Above the STBL a radiative flux divergence equal to  $\overline{w}ds_l/dz$  was specified to maintain the free-troposphere at a constant temperature despite a specified constant rate of divergence of  $D = 4 \times 10^{-6} \text{ s}^{-1}$ , which was chosen to yield a subsidence velocity of  $\overline{w}(z) \equiv -Dz \approx -0.32 \text{ cm s}^{-1}$  at cloud top.

The numerical discretization of the model was based on a mesh with 96 points in each horizontal direction and 400 points in the vertical, leading to a horizontal grid spacing of approximately 26 m and a vertical spacing of 3.75 m. Thus the domain had

a horizontal span of 2500 m and a vertical span of 1500 m. The model time step is determined dynamically to maintain stability. The simulation was run for approximately four hours of simulated time, with statistics being collected after the first hour.

Overall the simulated and observed cloud evolution were in satisfactory agreement. Cloud base in the LES descended at about a rate of  $6 \text{ m hr}^{-1}$  and cloud top rose at about  $2 \text{ m hr}^{-1}$ . Experiments designed to expose sensitivities to slight changes in the initial parameters and forcings (chosen to mimic uncertainty in radiative fluxes and initial state) and numerics (i.e., using a different vertical advection scheme) did not show marked sensitivities; thus the above level of agreement does not reflect a lucky choice of initial conditions and forcing, but seems to be robust.

However the LES did show a tendency to evolve away from the initially specified jump conditions. Maintaining the correct entrainment rates for the correct inversion layer structure proved difficult given our overly simplified approach to radiative transfer. For instance to maintain the correspondence between the simulated flow and the observed flow one would like the temperature structure above the boundary layer to be consistent with that observed. However, the observed value of  $T_l$  scales with  $(z - z_i)^{1/3}$  (cf., Eq. 8), thus an extra 8 m in the initial growth of the boundary layer is sufficient to increase the strength of the temperature jump by 2K (approximately 20 %) and reduce  $\kappa$  to 0.35. To mitigate this problem we initialized the boundary layer with slightly larger initial values of  $\kappa$  (weaker temperature jumps). Nonetheless, this difficulty was not eliminated, and there was some sense that the LES attempted to evolve toward a state in which its mixing lines were decidedly more neutral with respect to CTEI than those observed (cf., Fig. 6). To address these shortcomings requires careful experimentation with more realistic representations of radiative transfer (which given the size of the grid becomes very computationally demanding) and longer-time integrations wherein the turbulent evolution of the layer comes into a better balance with the air just above it. Although these types of experiments are beyond the scope of the present, predominantly observational, study it will be the focus of an upcoming study by the GEWEX (Global Energy and Water Experiment) Cloud Systems Studies Working Group 1.

In addition to matching the observed evolution of the cloud boundaries to within experimental uncertainty, the simulation plausibly represented at least some aspects of the observed energetics. This is illustrated in Fig. 9 where we show the measured and simulated profiles of vertical velocity variance,  $\sigma_w^2 \equiv \overline{w'w'}$ , and the skewness,  $S_w \equiv \overline{w'w'w'}/\sigma_w^{3/2}$ . Although, there are indications that the LES profile of  $\sigma_w$  varies more sharply with height than do the observed values, and that more of the observed variances is carried in scales larger than those that would fit in the LES domain, the overall magnitude of  $\sigma_w$  is about right. The LES derived profile of  $S_w$  agrees with the observations through most of the STBL, although it exhibits behavior in the upper part of the cloud layer which is uncharacteristic of the measurements. These failings are reminiscent of past evaluations (e.g., Moyer and Young, 1991; Moeng and Rotunno, 1990) and might be artifacts of the sub-filter model (note that no sub-filter estimates are available for  $S_w$ ), in which case they should be less evident as the LES filter length is reduced.

Despite lingering issues regarding the profiles of turbulent quantities near the flow boundaries, and the ability of the simulation to maintain a layer with the observed values of  $\kappa$ , the agreement between the LES and the data was better than expected. This might, however, merely be a statement of the extent to which our expectations had been lessened by the apparent discord among previous LES. Because LES is not expected to (and shows no evidence of) effectively representing the detailed processes occurring

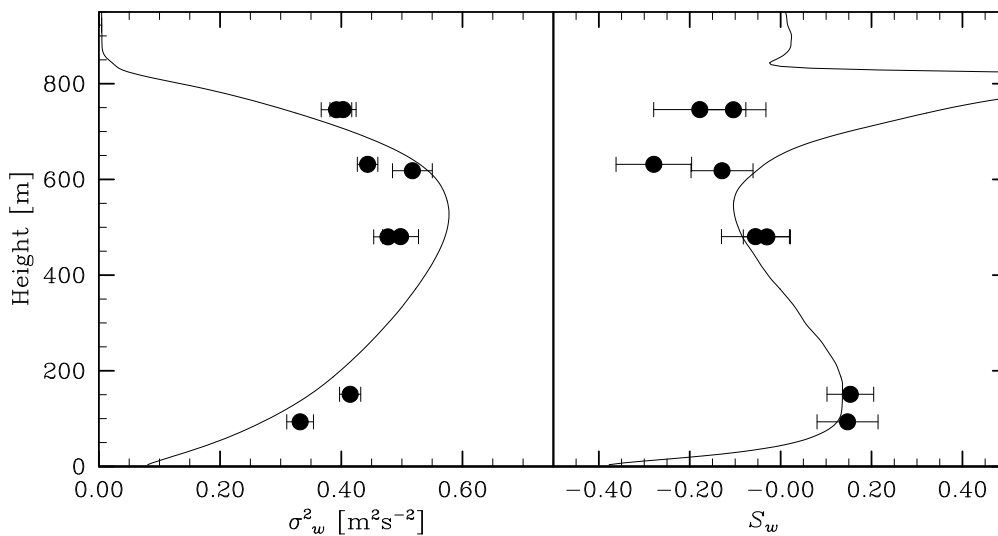


Figure 9. Plot of vertical velocity variance (resolved plus sub-filter estimate) from LES, and that derived from flights (left panel) and skewness (right panel). Flight-data shows mean variance and standard deviations for 2.5 min (15 km) sub-legs of 30 minute legs.

at cloud top, these results are encouraging for the method, and to some extent support the idea that the detailed entrainment rate is controlled by macroscopic, or large-eddy processes (e.g., Lewellen and Lewellen 1998). To the extent that these results can be reproduced with flow solvers using different numerics, or more detailed representations of radiative processes, or for other flights during DYCOMS-II, they provide a rational basis for investigating how entrainment depends on a variety of parameters.

## 6. SUMMARY AND CONCLUSIONS

After corrections for non-Lagrangian effects, data collected during the first research flight of DYCOMS-II show evidence of a stable to deepening cloud layer despite macroscopic conditions thought to favor cloud dissolution through CTEI. Best estimates show cloud base lowering at a rate of several meters per hour, the evolution of cloud top is difficult to discern from its spatial variability except to say that it is not changing markedly. Comparisons of the STBL and free-tropospheric states yield a value of the CTEI stability parameter,  $\kappa$  of approximately 0.45; significantly larger than the critical value of 0.23 thought to portend the breakup of the cloud layer. Although past observations have indicated that  $\kappa > 0.23$  is not a sufficient condition for the dissolution of the cloud layer, recent modeling studies have rehabilitated  $\kappa$  as a measure of cloud longevity. Observations during RF01 do not support this point of view.

The observations are also used to make five quasi-independent estimates of entrainment. Each of these estimates is broadly consistent with the others and contribute to a best estimate of the entrainment rate of  $E \approx 0.4 \pm 0.1$  cm s<sup>-1</sup>. The relatively small value of uncertainty which derives from the consistency of the multiple estimates allows meaningful tests of entrainment rules. Of the five rules tested, two perform poorly and three are plausible. The three plausible rules show markedly different sensitivities to environmental parameters such as surface latent heat fluxes, radiative forcing and values

of  $\kappa$ , thus encouraging the use of data from other flights to further discriminate among rules.

LES was also evaluated against the RF01 data. It was found to well reproduce the macroscopic evolution of the cloud layer, although in so doing it had difficulty in maintaining the observed inversion layer structure. Because it is uncertain what role detailed radiative processes play in this aspect of the simulation further work is necessary using LES with more accurate representations of long-wave radiative transfer. Higher resolution simulations are also necessary to evaluate what appear to be systematic biases in the representation of the structure of the vertical velocity field near cloud top. Overall however the ability of LES to represent the macroscopic evolution of the layer was encouraging, and suggests that the method might be usefully employed to help further discriminate among entrainment rules.

#### ACKNOWLEDGEMENT

The authors would like to acknowledge the many contributions of the engineers, management, pilots, mechanics, and scientists of the Research Aviation Facility and the staff of North Island Naval Air Station who helped facilitate the collection of data during DYCOMS-II. The lead author would also like to acknowledge discussions with Margreet van Zanten, the contributions of Dave Leon in the analysis of the Radar data, the help of Verica Savic-Jovcic in processing the dropsonde data, and discussions regarding entrainment with David Lewellen. Support by the National Science Foundation, through Grant # ATM 0097053 is also gratefully acknowledged. Lastly, Roddy Rogers of NSF and Dave Carlson of NCAR-ATD are thanked for their support and encouragement.

#### APPENDIX A

##### *Data*

The distribution of flight time with altitude during RF01 is illustrated in Fig. A.1. With the exception of the leg skimming cloud top (whose latter half incidentally revealed the one instance of a moist layer intersecting cloud top), all level legs were approximately 30 minute circles, flown in alternating CW and CCW directions. For purposes of data analysis the aircraft altitude and roll angle were inspected on all the legs and only those times when the aircraft altitude did not vary significantly (more than  $\pm 10$  m from the mean ) and the roll angle fluctuated less than a couple of degrees (mean roll angles were about  $\pm 2^\circ$  for circular legs of radius 30 km) were selected for further analysis. This selection results in the segmentation of flight data tabulated in the electronic supplement of Stevens *et al.*, (2002).

During DYCOMS-II temperature estimates are based on measurements from one of three standard temperature probes. Two of these (ATRR and ATRL) were Rosemount 102E2AL probes mounted on the left and right side of the fuselage. Both have a stated accuracy of 0.5 K. The third probe (ATWH) was a wing-mounted Rosemount 102E de-iced probe. It has about twice the error of the 102E2AL. A comparison of the ATRR and ATRL signals indicated a slight drift on two legs toward the beginning of the flight. Further comparisons with ATWH indicated that the source of the drift was the ATRL probe. Thus all the data in this paper is based on the ATRR probe. Because the Research Aviation Facility used ATRL as the base temperature probe, some amount of reanalysis on derived variables was necessary to use ATRR during RF01. On legs where there was no evidence of drift between ATRR and ATRL a comparison of the two showed little indication of wetting effects in the cloud leg.

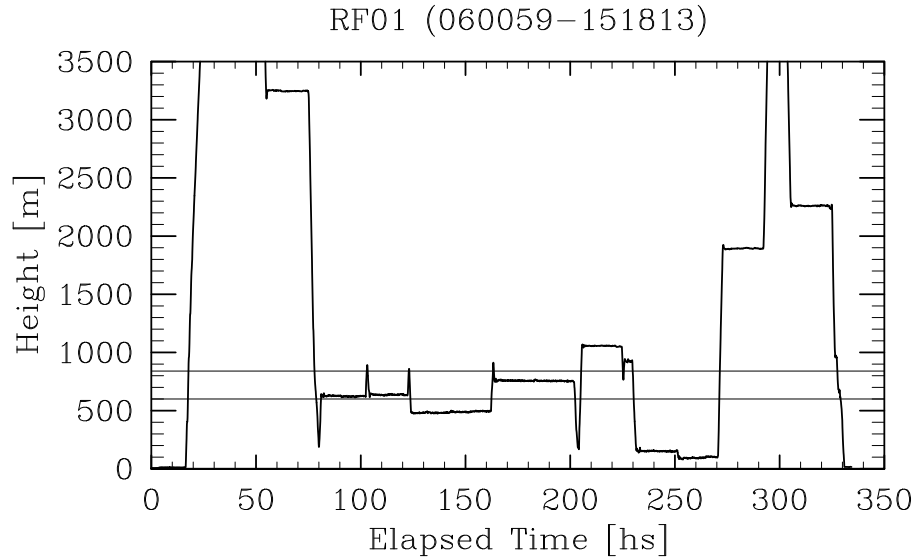


Figure A.1. Altitude versus time for RF01

Humidity data was collected with five probes during DYCOMS-II. Two thermo-electric dew-point hygrometers (General Eastern Instruments 1011B), which were mounted on the top and bottom of the fuselage, provided slow (order minute) estimates of atmospheric humidity. Fluctuations were measured with cross-flow and stub Lyman- $\alpha$  hygrometers. Generally the cross-flow instrument is thought to be less susceptible to wetting. In addition, a laser hygrometer (the TDL, or tuneable diode laser) was flown. In principle the TDL can yield absolute high-rate measurements of humidity, but the data are not yet available. Inspection of the Lyman- $\alpha$  outputs indicated superior frequency response for the cross-flow instrument (MRLA1) and thus it was used in analyses which required fast hygrometer data. When slow data was necessary (i.e., for estimating leg means) the dew-point measurements from the bottom hygrometer were used, because when compared to the measured temperature in cloud legs this instrument performed better. A comparison of all the humidity probes with the saturation humidity as derived from temperature measurements in cloud indicated considerable scatter. Because of the close correspondence between temperature probes (particularly at high-frequencies) this scatter was attributed to wetting of the humidity sensors. Hence for mean state estimates the humidity along in-cloud legs was derived by assuming saturation at the measured temperature.

In our analysis all the liquid water data were taken from the PVM-100 probe. In general its values compared favorably with measurements made with the PMS/CSIRO hot-wire probes (i.e., the King Probe) mounted on the wings.

To improve the accuracy of the dew-point hygrometers the difference between saturation specific humidity and the specific humidity as measured by the probes was plotted as a function of measured cloud water during cloud legs. This analysis indicated an offset of about  $0.25 \text{ g kg}^{-1}$  for the dew-point hygrometer versus  $q_s$  comparison

and an offset of about  $0.30 \text{ g kg}^{-1}$  when the comparison was made with the Lyman- $\alpha$ . These offsets are within the stated accuracies of the instruments. In principle the offset could be attributed to either the temperature or the humidity measurements (i.e., leading to colder and drier estimates of the STBL state), but because of the seemingly poorer performance of the humidity instruments we corrected these for the presumed bias. These corrections, based only on in-cloud data, led to better global agreement between cloud base (as measured from lidar, Graham Feingold personal communication 2002, and from vertical soundings) and lifting condensation level as calculated along all boundary layer legs.

Downward and upward long-wave ( $3.5\text{-}50 \mu$ ) radiative fluxes were measured with upward and downward looking Eppley Pyrgeometers. These instruments require calibration and have no stated absolute accuracy. In our comparisons with calculated radiative fluxes, “eye-estimated” offsets of  $17 \text{ W m}^{-2}$  and  $14 \text{ W m}^{-2}$  were added to the downward and upward measured fluxes respectively to yield better agreement with calculated fluxes based on the mean state. Past experience (Krista Laursen, personal communication 2002) indicates that such adjustments are reasonable. Moreover since all of the analysis in this paper depends on differences in the net flux with height, the addition of a constant offset to the flux has no impact.

Surface temperatures were estimated using two Heimann Infrared (KT19.85) Radiometric Bolometers. Generally they agreed to much better than the stated accuracy of the instrument (0.5 K), although they indicated temperatures consistently 0.5 K warmer than satellite derived estimates.

Lidar derived cloud top heights were determined by the maximum return signal in the range interval where the cloud top is expected. The intent of using a range interval was to eliminate the near field return which could give false cloud top measurements on flight legs very near cloud top. Lidar range was converted into cloud top height using the aircraft altitude, and correcting for additional range dilation associated with aircraft roll angles. Offsets in range based aircraft altitude and aircraft altitude were also applied when surface returns were available. Overall the differences between IR and green wavelength cloud top heights were not found to be significant, and the accuracy of the lidar derived cloud top heights is estimated as  $\pm 1$  range bin, equivalently  $\pm 3.75$  m.

DMS was measured by an atmospheric pressure ionization mass spectrometer (APIMS) developed at Drexel University (Bandy *et al.*, 2002). Protonation of DMS is achieved by hydronium ions and clusters at near ambient pressures. Sampling of the mass peak at  $\text{DMSH}^+$  and isotopically labeled DMS takes place each at 25 Hz.

Ozone was measured using a reverse chemiluminescence technique built at NCAR’s Research Aviation Facility (RAF) in 2001 and is very similar to that documented in Pearson and Stedman (1980). Continuous in-flight calibration is maintained by running a slower response UV photometric (Thermo Environmental Instruments) analyzer in parallel. The minimum detection limit of the fast instrument is estimated to be less than 0.075 ppbv in one second; however the accuracy, as tied to the slower response instrument which is in turn calibrated against a transfer standard, is  $\pm 1$  ppbv. The nominal bandwidth of the chemiluminescence instrument is near 10 Hz, limited by the residence time of the air sample within the detection chamber. A more thorough discussion of the instrument performance and the cospectral behavior of the scalar fluxes may be found in a forthcoming manuscript (Faloona *et al.*, in preparation, 2002).

Turbulent fluxes were calculated using 2.5 minute ( $\approx 15$  km) sub-segements over which the tracer and the velocity field were demeaned and detrended. The length of the interval was settled upon after a perusal of many scalar/vertical wind speed

cospectra. Nonetheless, it is somewhat arbitrary and does moderately affect the fluxes. However, inspection of the cospectra appeared to reveal that this filter cutoff does not systematically bias the fluxes (that is sometimes the larger scales contribute positively and sometimes negatively), so the error is somewhat accounted for in the scatter of the fluxes.

## APPENDIX B

### *Error Estimates*

Errors were estimated using standard methods (e.g., Bevington 1969, or Taylor, 1982). For instance, the uncertainty in the estimate of an expression  $f(x_1, x_2, \dots, x_n)$  is denoted  $\sigma_f$  and is estimated as

$$\sigma_f^2 = \sum_{i=1}^n \left( \frac{\partial f}{\partial x_i} \sigma_{x_i} \right)^2, \quad (\text{B.1})$$

which assumes that the uncertainties in the  $x_i$ 's are independent. This form of calculations was used to propagate errors in estimates such as Eq. 10 and 11, as well as estimates of  $E$  using the ratio method, or in estimates of the surface fluxes derived from the bulk flux algorithm.

In all cases the individual component errors which make up the total error in the final entrainment estimate were assumed to be independent. In the final calculation of entrainment based on the jump and the flux at the inversion (Eq. 5), one has grounds to make other arguments. Since we have reason to believe that the thermodynamic environment and the entrainment velocity is relatively uniform across the horizontal scales of the experiment, it follows that the magnitude of the scalar flux at the cloud top is correlated with its jump. We estimate this covariance term from the observed spatial correlation between the individual 150 s flux measurements and the absolute scalar concentration within the STBL (assuming that the concentration aloft is constant) and considered its inclusion in the flux estimates according to

$$\sigma_E^2 = \left( \frac{\sigma_\Delta}{\Delta} \right)^2 + \left( \frac{\sigma_\psi}{\psi} \right)^2 - 2 \left( \frac{\sigma_\Delta}{\Delta} \right) \left( \frac{\sigma_\psi}{\psi} \right). \quad (\text{B.2})$$

This correction was easiest to make for DMS because the jump is always equal to the mean concentration and thus can be measured simultaneously with the flux. For this reason the correction was only applied for DMS. It resulted in a reduction of our estimated error from  $0.15 \text{ cm s}^{-1}$  (without the covariance term) to the stated value of  $0.08 \text{ cm s}^{-1}$ .

Estimates of the uncertainty of a flux profile were derived by fitting lines of the form||

$$\hat{\psi} = \psi_* + b(z - z_*) \quad (\text{B.3})$$

with  $z_* = 0$  and  $z_* = z_i$  to the  $n$  data pairs  $(z_i, \psi_i)$ . For a given  $z_*$  we estimate the uncertainty in the intercept as

$$\sigma_{\psi_*}^2 = \frac{\sum_{i=1}^n w_i z_i^2}{\sum_{i=1}^n w_i \sum_{i=1}^n (w_i z_i^2) - (\sum_{i=1}^n w_i z_i)^2}. \quad \text{where } w_i = \sigma_{\psi_i}^{-2}. \quad (\text{B.4})$$

|| Strictly speaking this was only done for scalars for which  $F$ , the non-turbulent flux, vanished, and for which  $S$  was either negligible or constant throughout the STBL. Because  $s_l$  does not satisfy this requirement we actually fit a line to the sum of  $\psi_{s_l}$  and  $F_{lw}$ .

We then bound our estimate of the flux by the rhomboid defined by uncertainty in the surface and cloud top (e.g.,  $z_i$ ) intercepts. To estimate  $\sigma_{\psi_i}$ , the uncertainty of the flux at some height  $z_i$ , in the above expression we calculate an intrinsic uncertainty,  $\sigma_{\psi_i|t}$  due to turbulent fluctuations using the integral scale of the quantity whose flux we are interested in (e.g., following Mann and Lenschow, 1994) and a meso-scale uncertainty associated with measuring fluxes at different times, or possibly in different regions. This meso-scale uncertainty is estimated from our fit as:

$$(\sigma_{\psi|m})^2 = \frac{1}{n-2} \sum_{i=1}^n (\hat{\psi} - \psi_i)^2. \quad (\text{B.5})$$

Assuming that the turbulence and mesoscale contributions to the error are independent leads us to conservatively estimate  $\sigma_{\psi}^2 = (\sigma_{\psi|m})^2 + (\sigma_{\psi_i|t})^2$ .

The jumps in scalar quantities appear repeatedly in our equations. To estimate the jumps in  $\text{O}_3$ ,  $q_t$  and  $s_l$  we use a mixing diagram, and errors in the jumps are estimated using a combination of the mean values in the STBL and in the above cloud legs. One advantage of DMS in this regard is that because it is zero above the STBL the uncertainty in its jump is just the uncertainty in its mean STBL value.

#### REFERENCES

- Bandy, A.R., D.C. Thornton, F.H. Tu, B.W. Blomquist, W. Nadler, G.M. Mitchell, and D.H. Lenschow 2002 Determination of the vertical flux of dimethyl sulfide by eddy correlation and atmospheric pressure ionization mass spectrometry (APIMS), *J. Geophys. Res.*, in press.
- Bretherton, C. S., M. MacVean, P. Bechtold, A. Chlond, W. Cotton, J. Cuxart, H. Cuijpers, M. Khairoutdinov, B. Kosovic, D. Lewellen, C.-H. Moeng, P. Siebesma, B. Stevens, D. Stevens, I. Sykes and M. Wyant 1999 An intercomparison of radiatively-driven entrainment and turbulence in a smoke cloud, as simulated by different numerical models. *Quart. J. Roy. Meteor. Soc.*, **125**, 391–423.
- Bevington 1969 *Data reduction and error analysis for the physical sciences*, McGraw-Hill, New York
- Deardorff, J. W. 1980 Cloud top entrainment instability. *J. Atmos. Sci.*, **37**, 131–147.
- Gerber, H., S. P. Malinowski, J.-P. Brenguier and F. Burnet 2002 On the entrainment process in stratocumulus clouds. Preprints, *11th Conf. On Cloud Physics*, Ogden, UT, Amer. Meteor. Soc., CD-ROM, JP7.6
- Fairall, C. W., E. F. Bradley, D.P. Rogers, J.B. Edson, and G. S. Young 1996 Bulk parameterization of air-sea fluxes for tropical ocean global atmosphere coupled-ocean atmosphere response experiment *J. Geophys. Res.*, **101**, 3747–3764.
- Fu, Q., and K.-N. Liou 1993 Parametrization of the radiative properties of cirrus clouds, *J. Atmos. Sci.*, **50**, 2008–2025.
- Kawa, S. R. and R. Pearson Jr. 1989 An observational study of stratocumulus entrainment and thermodynamics. *J. Atmos. Sci.*, **46**, 2649–2661.
- Kuo, H.-C. and W. Schubert 1988 Stability of cloud-topped boundary layers. *Quart. J. Roy. Meteor. Soc.*, **114**, 887–916.
- Lenschow, D. H., P. B. Krummel and S. T. Siems 1999 Measuring entrainment, divergence, and vorticity on the meso-scale from aircraft. *J. Atmos. Oceanic Tech.*, **14**, 1384–1400.
- Lewellen, D. and W. Lewellen 1998 Large-eddy boundary layer entrainment. *J. Atmos. Sci.*, **55**, 2645–2665.
- Lilly, D. K. 1968 Models of cloud topped mixed layers under a strong inversion. *Quart. J. Roy. Meteor. Soc.*, **94**, 292–309.
- Lilly, D. K. 2002 Entrainment into cloud-topped mixed layers: A new closure. *J. Atmos. Sci.*, in press.
- Lock, A. P. 1998 The parameterization of entrainment in cloudy boundary layers. *Quart. J. Roy. Meteor. Soc.*, **124**, 2729–2753.
- Lock, A. P. and M. K. MacVean 1999 The generation of turbulence and entrainment by buoyancy reversal. *Quart. J. Roy. Meteor. Soc.*, **125**, 1017–1038.

- Mann, J. and D. H. Lenschow 1994 Errors in airborne flux measurements. *J. Geophys. Res.*, **99**, 14,519–14,526.
- Moeng, C.-H. 2000 Entrainment rate, cloud fraction and liquid water path of PBL stratocumulus clouds. *J. Atmos. Sci.*, **57**, 3627–3643.
- Moeng, C.-H. and R. Rotunno 1990 Vertical–velocity skewness in the buoyancy-driven boundary layer. *J. Atmos. Sci.* **47** 1149–1162.
- Moeng, C.-H. and co authors 1996 Simulation of a stratocumulus-topped PBL: Intercomparison among different numerical codes. *Bull. Amer. Meteor. Soc.*, **77**, 261–278.
- Moeng, C.-H., P. P. Sullivan and B. Stevens 1999 Including radiative effects in an entrainment-rate formula for buoyancy driven PBLs. *J. Atmos. Sci.*, **56**, 1031–1049.
- Moyer, K. A. and G. S. Young 1991 Observations of vertical velocity skewness within the marine stratocumulus-topped boundary layer. *J. Atmos. Sci.*, **48**, 403–410.
- Phillips, O. M. 1966 *The dynamics of the upper ocean*, Cambridge University Press, Cambridge, 261 pp.
- Pearson, R. Jr and D. H. Stedman 1980 Instrumentation for fast response ozone measurements from aircraft, *Atmos. Tech.*, **12**, 51–55
- Randall, D. A. 1980 Conditional instability of the first kind upside-down. *J. Atmos. Sci.*, **37**, 125–130.
- Russell, L. M., D. H. Lenschow, K. K. Laursen, P. B. Krummel, S. T. Siems, A. Bandy, D. Thornton and T. S. Bates 1998 Bidirectional mixing in an ACE-1 marine PBL overlain by a second turbulent layer. *J. Geophys. Res.*, **103**, 16411–16432.
- Turton, J. D. and S. Nicholls 1987 A study of the diurnal variation of stratocumulus using a multiple mixed layer model. *Quart. J. Roy. Meteor. Soc.*, **113**, 969–1009.
- Schubert, W. H., J. S. Wakefield, E. J. Steiner and S. K. Cox 1979 Marine stratocumulus convection. Part II: Horizontally inhomogeneous solutions. *J. Atmos. Sci.*, **36**, 1308–1324.
- Stevens, B. 2002 Entrainment in Stratocumulus Topped Mixed Layers *Quart. J. Roy. Meteor. Soc.*, **128**, XXX.
- Stevens, B. and Co-Authors 2002 Dynamics and Chemistry of Marine Stratocumulus – DYCOMS-II *Bull. Amer. Meteor. Soc.*, **83**, XXX.
- Taylor, J. R. 1982 *An introduction to error analysis : the study of uncertainties in physical measurements*, University Science Books, Mill Valley CA,
- Turton, J. D. and S. Nicholls 1987 A study of the diurnal variation of stratocumulus using a multiple mixed layer model. *Quart. J. Roy. Meteor. Soc.*, **113**, 969–1009.
- Vali, G., R. D. Kelly, J. French, S. Haimov, D. Leon, R. E. McIntosh and A. Pazmany 1998 Finescale structure and microphysics of coastal stratus. *J. Atmos. Sci.*, **55**, 3540–3564.